Role of Hydrophilicity and Length of Diblock Arms for Determining Star Polymer Physical Properties

Lisa E. Felberg[1], David H. Brookes[3], Teresa Head-Gordon[1-4*]

[1]Department of Chemical and Biomolecular Engineering, [2]Department of Chemistry, [3]Department of

Bioengineering, University of California Berkeley,

Berkeley, California 94720, USA

[4]Chemical Sciences Division, Lawrence Berkeley National Labs

Berkeley, California 94720, USA

Julia E. Rice[5] and William C. Swope[5*]

[5]IBM Research, IBM Almaden Research Center

San Jose, California 95120, USA

*Corresponding authors

Email: thg@berkeley.edu

ABSTRACT

We present a molecular simulation study of star polymers consisting of 16 diblock copolymer arms bound to a small adamantane core, by varying both arm length and the outer hydrophilic block when attached to the same hydrophobic block of poly-δ-valerolactone (PVL). Here we consider two biocompatible star polymers in which the hydrophilic block is composed of polyethylene glycol (PEG) or poly-methyloxazoline (POXA), in addition to a polycarbonate-based polymer with a pendant hydrophilic group (PC1). We find that the different hydrophilic blocks of the star polymers show qualitatively different trends in their interactions with aqueous solvent, orientational time correlation functions, and orientational correlation between pairs of monomers of their polymeric arms in solution, in which we find that the PEG polymers are more thermosensitive compared to the POXA and PC1 star polymers over the physiological temperature range we have investigated.

KEYWORDS

INTRODUCTION

Star polymers are globular nanoparticle architectures in which linear polymer "arms" are connected to a central polymer core. Recent advances in the ease of their synthesis has created the possibility of realizing a large combinatorial variation in the structure and function of these nanoparticles through the patterning of chemical functional groups and/or the length of the polymeric arms[1, 2]. However, synthetic advances made on star polymers have far out-paced the corresponding physical characterization of their structural, thermodynamic, or dynamical properties, and thus the ability to rationally navigate the vast chemical landscapes of possibilities for creating a useful star polymer. For example, a particular functional goal is to develop a star polymer capable of serving as a molecular drug-delivery vehicle, which therefore adds additional design restraints for safe performance under physiological conditions of temperature and aqueous solvent[3].

In a recent paper, some of us have performed all atom explicit solvent molecular dynamics simulations of three different star polymeric systems in water at physiological temperatures[4]. In this previous star polymer comparison, the diblock arms consisted of an inner "hydrophobic" block which was varied in the three systems to be either polylactide, poly-δ-valerolactone (PVL), or polyethylene, while holding the outer hydrophilic block fixed to the same polyethylene glycol (PEG) polymer that is widely used as an *in vivo* biomaterial. (We note that PEG versus PEO is a matter of size, with smaller MW polymers being referred to as PEG while larger ones are called PEO, with a cutoff that is usually around 20,000 Daltons; we are below this threshold and hence refer to them as PEG star polymers). It was determined that the hydrophobic regions of these systems were very glassy, but it was speculated that this could be an artifact that is due to the small and structured adamantane core to which they are directly attached, and perhaps the small sizes of star polymers that were simulated. Furthermore, a sharp boundary existed between the hydrophobic cores and outer block of water solubilized PEG at low temperatures, although solubility as measured by surface area contact of the polymer arms with water decreased as the temperature was increased. This might suggest the presence of a lower critical

solution temperature (LCST) for the PEG star polymer, which is known to exist for linear PEG−water mixtures[5], suggesting that through design such polymers could be thermally responsive in a temperature regime useful for physiological applications.

Here we present a comparative simulation study of how the physical properties of the model star polymers change by now holding the inner hydrophobic PVL block (attached to the adamantane core) fixed, but now varying the outer block hydrophilic monomer as either PEG, poly-methyloxazoline (POXA), or a polycarbonate-based polymer with a pendant hydrophilic group (PC1). The introduction of POXA adds additional hydrogen bonding sites beyond the basic PEG ester group, while PC1 adds yet an additional feature of polymer branching. We also compare doubling the length of the hydrophobic PVL block to assess possible artifacts introduced by the adamantane core, as well as significantly elongating the hydrophilic blocks compared to the previous study. These new comparisons of chemical features and size are explored to understand what drives star polymer thermally induced structural changes, especially in regards to questions on how cargo is held or released, or the exposure of sites to hydrolysis reactions that promote biodegradation, all of which are important factors relevant to their suitability as a drug delivery material.

METHODS AND MODELS

Molecular systems: Each of the polymer systems was created by connecting 16 diblock polymer arms to a central adamantane molecule. Adamantane, $C_{10}H_{16}$, is comprised of 10 carbon atoms in a diamond lattice structure. Each hydrogen site of the adamantane was removed and used as a connection site for the hydrophobic end of a diblock arm. The hydrophobic chain was connected to a hydrophilic chain, completing the diblock arm. Each of the four polymers studied had the same hydrophobic region chemistry of a block polymer created from the monomer δ-valerolactone, which will be referred to as PVL. The varying hydrophilic regions were designed to represent a range of molecular features

including various degrees of hydrogen-bonding and branching, as well as arm length variation. Figure 1 provides an example of the representative features of the diblock star polymers evaluated here.

The arm chemistry of the first polymer consists of eight units of PVL connected to a hydrophilic region of six repeat units of ethylene oxide to form PEG; it will be referred to throughout the paper as PVL_8PEG_6 or S-PEG (S for short). This nomenclature refers both to the arms that make up the star polymer as well as to the star polymer made from those arms. The second polymer consists of eight units of PVL connected to a hydrophilic region of six repeat units of dimethylacetamide to form poly-oxazoline, POXA; experimentally, the polymer POXA is created from a ring-opening polymerization of the compound oxazoline, which is the origin of its name. It will be referred to throughout the paper as PVL_8POXA_6 or S-POXA. The number of monomer units of the hydrophilic regions of PVL_8PEG_6 and PVL_8POXA_6 were selected to yield approximately equal arm lengths when the two star polymer arms are fully extended. The third polymer is chemically related to the first, comprised of sixteen units of PVL connected to a hydrophilic region of twenty-four repeat units of ethylene glycol; it will be referred to throughout the paper as $PVL_{16}PEG_{24}$ or L-PEG (L for long). The fourth polymer is also composed of longer arms, comprising sixteen units of PVL connected to a hydrophilic region of twelve repeat units of a functionalized methyl propyl carbonate to form the polymer PC1; it will be referred to throughout the paper as $PVL_{16}PC1_{12}$ or L-PC1. Again, the number of monomer units of the hydrophilic regions of $PVL_{16}PEG_{24}$ and $PVL_{16}PC1_{12}$ were selected to yield approximately equal arm lengths when the two star polymer arms are fully extended. A summary of each polymer and their monomeric chemical structure is given in Table 1.

Force fields: The force fields used for water, PVL, and PEG have been described thoroughly in a previous publication[3, 4], which we briefly summarize here. We used the TIP4P-Ew[6] as the model for aqueous solvent in all simulations performed in this study. For the adamantane core and the linkage of adamantane to the hydrophobic chain of PVL, OPLS-AA parameters[7] were used but with improved parameters of Price et al.[8] for the alkane torsion angle energy expressions. Our previous study carefully

5

For the polyoxazoline segments of each arm, the repeat unit is $-CH_2-N(CO-CH_3$ [3]$)-CH_2-$, with parameters expected to be like those for N,N-dimethylacetamide, but with charges modified so that repeat units are charge neutral. For polyoxazaline chains, the OPLS-AA atom types are -CT-N-CT along the backbone, with HC as the atom type for hydrogen on backbone carbon aliphatic CT sites, and N (amide) for the nitrogen. The polyoxazaline side chain is a methoxy group ($-CO-CH_3$) with OPLS-AA atom types C and O for the carbonyl group and CT and HC for the terminal methyl sites. Charges are +0.06 for all HC sites and +0.06 for the backbone CT sites; the N sites have charge -0.36; C of the carbonyl groups have charges of +0.60 and O of the carbonyl groups have charges of -0.60; CT on methyl groups at the end of the sidechains have charges of -0.18. At the end of each arm, there is a terminal methyl group with a charge on the carbon sites set to 0.00; the three hydrogen atoms on that site make the last repeat unit charge neutral. Bond, angle and torsion parameters for the polyoxazoline segment were OPLS-AA parameters from the literature[7-15], and especially from Price, et al.[8], who report parameters for esters and hydrocarbons. The parameter set did not include parameters for torsions with atom types CT-N-CT-CT, so values for type CT-N-CT-HC were substituted. For linkages between the polyoxazoline and polyvalerolactone segments, parameters for ethyl propanoate were used from Price, et al[8]. OPLS-AA parameters in the current literature also do not include parameters for torsions with atom types N-CT-CT-N, so values for NT-CT-CT-NT (NT for amine nitrogen) were substituted.

The repeat units on the PC1 hydrophilic segments are $-CR(CH_3)-CH_2-O-CO-O-CH_2-$ and the side chain on each repeat unit is R=$-CO-NH-CH_2-CH_2-OH$. Propylmethyl carbonate (PMC) and dimethyl carbonate (DMC) were studied as model molecules for the determination of parameters for the repeat units along the polycarbonate backbone for the hydrophilic segment. OPLS-AA atom types

for the carbonate were chosen to be similar to esters, namely CT for the methyl and propyl aliphatic carbon sites, HC for the corresponding hydrogen sites; OS for the ether-type backbone oxygen sites, C for the backbone carbonyl carbon and O for the carbonyl oxygen. These OPLS-AA atom types determine the Lennard-Jones parameters and most of the bonded parameters (bond, angle and torsion parameters) consistent with those for esters.

Charges for the carbonate group sites were taken from an analysis of charges used for DMC by other force fields, from ESP fits to electrostatic potentials produced from gas phase quantum chemical calculations, as well as solution phase (PCM) quantum chemical calculations using continuum representations of either liquid water or dimethyl carbonate (DMC), with a dielectric constant of approximately 3, as solvent. The quantum chemical approach was based on structures optimized using MP2 (aug-ccpVTZ), after which B3LYP DFT calculations were performed using PCM models for the solvent. Electrostatic potentials were fitted using software developed in house at IBM that supports constraints on total charge as well as to establish charge equivalence among sets of sites. Although there were small variations among methods, the results were surprisingly consistent. Moreover, there was not much change in these charges as a function of the OCOC torsion angle. Consistency of charge model with respect to solvent environment and molecular structure suggests that a fixed charge model for carbonates might be adequate for many purposes.

For use in polymeric material we required a charge model that produced charge neutral groups and could be used in the context of material described by other OPLS-AA parameters. The charges in Table 2 for DMC are the result. These result in a charge of -0.414 for the –O-CO-O- carbonate functional group, which is then balanced by net charges of +0.207 on the alpha methylene groups on each side of it. These methylene groups have a charge of +0.105 on the (CT) carbon sites and +0.051 on the (HC) hydrogen sites. Changing the number of hydrogen sites bonded to this alpha carbon would change its charge by 0.051 for each hydrogen added or removed in order to maintain a net charge of +0.207 on groups alpha to the carbonate. Although the local charge density on the carbonyl group is

more polar than for esters, the rest of the charges are similar. Simulations of pure liquid DMC using these parameters (not shown) give adequate densities.

Given this charge model and ester-like atom types, all of the Lennard-Jones, bond and angle parameters and most of the torsion parameters for a polycarbonate backbone can be found in the OPLS force field literature. There are a few exceptions. Angle terms involving OS-C-OS bending were missing. We used an equilibrium angle of 113.2 degrees to be compatible with the O-C-OS equilibrium angle of 123.4 degrees, in order to allow the four sites of the carbonate region to lie flat. A few torsion parameters were missing: for CT-CT-CT-OS we substituted parameters for CT-CT-CT-CT, since these have similar multiplicity and barrier height. For torsions involving atom types CT-OS-C-OS, we used parameters developed by Gontrani, et al.[16], for their modeling of DMC. This energy term produces a barrier that helps the molecule maintain the preferred trans-trans conformation, i.e., a "w" shape, over the cis-trans form. Note that starting from OPLS-AA parameters, Gontrani, et al.[16] made other modifications, but we are using only their torsion parameters for this particular torsion type.

For polycarbonate chains beyond DMC, a very important torsion is that described by CT-CT-OS-C, since this is the first "floppy" torsion beyond the relatively rigid DMC ($-CH_2$-O-CO-O-CH_2-) group within a polycarbonate polymer. Parameters exist for this kind of torsion energy term in the OPLS-AA force field for esters groups. We used these parameters with the OPLS-AA atom types, the charge model and modifications described above, to produce an energy curve as a function of torsion angle from a series of constrained optimizations on propyl methyl carbonate, where each optimization was performed with a different constrained value of the CT-CT-OS-C torsion angle. The resulting energy curve showed three nearly degenerate minima, one at the expected value of 180 degrees (trans), and two others near +/-80 degrees, with a barrier between them of about 1 kcal/mole. This energy curve was compared with a similar one produced from calculations performed in the gas phase using an MP2/auc-ccpVTZ level of theory (Figure 2). The quantum calculations showed the trans structure to be the most stable, but with two very shallow minima (almost shoulders) at +/-90 degrees, and they

were 1.5 kcal/mole higher in energy than the trans structure. We felt compelled to fix this error in our version of the force field since the presence of these two spurious minima would affect the persistence length and conformational preferences of the polycarbonate chains. Therefore, we developed new parameters for the CT-CT-OS-C torsion by fitting to the quantum result. The resulting three term fit, U(phi)=0.3693 *(1+cos(phi)) + 0.2342*(1-cos(2*phi)) + 0.1315*(1+cos(3*phi)) (all units are kcal/mole) did an excellent job at reproducing the quantum energy curve.

The hydrophilic sidechain attached to the carbonate backbone consists of an amide group, a short ethyl chain and an alcohol group. OPLS-AA parameters for these chemical groups are well established since they are components of peptides and other well studied organic molecules. OPLS-AA atom types and charges are C (carbonyl Carbon, +0.5), O (carbonyl Oxygen, -0.5), N (amide Nitrogen, -0.5), HN (amide hydrogen, +0.3), CT (+0.08) and HC (+0.06) for the methylene group near the amide, CT (+0.145) and HC (+0.06) for the methylene near the hydroxyl group, and OH (-0.683) and HO (+0.418) for the hydroxyl group. Note that the side chain is charge neutral. OPLS-AA parameters for the Lennard Jones and bond terms for the side chain are from the literature.

Simulation Protocol: The initial configurations for all four star polymers were developed with in-house software. The star polymers are created in a fully extended state, with end-to-end distances as long as 204 Å. These extended structures were partially collapsed *in vacuo* after a short energy minimization, in which the collapsed structures ranged from 48 to 70 Angstroms in diameter. A cubic box of 46,656 TIP4P-Ew[6] water molecules was prepared and equilibrated using locally developed software and a protocol previously described[6] with a control temperature of 300 K and an external pressure of 1 atm. A set of bulk water coordinates was obtained from the resulting simulation (box edge length 111.9453 Å) representing an instantaneous density of 0.9949 g/cm^3, in excellent agreement with experimental values.

The starting conformation for the simulations of solvated star polymers was constructed as follows: (1) The coordinates of the partially collapsed star polymer sites were translated so that the

center of geometry was at the center of the cubic box from the water simulation. (2) For each water molecule, the smallest distance from any of its three sites to any of the polymer sites was computed. (3) Using these distances, water molecules were removed from the simulation, beginning with the closest water and then the second closest and so on, until the total mass of the removed water molecules just exceeded the total mass of the star polymer. Depending on the size and type of star polymer, between 954 and 3,598 water molecules were removed by this procedure. By construction, each solvated star polymer system has the same volume and nearly the same mass, hence the same mass density, as that of water. With the closest water molecules removed in this way, dynamical simulations could be started without any additional preparation.

Simulations were performed using a version of the LAMMPS software[17] dated April 2012. Molecular dynamics simulations were performed on an IBM BlueGene/L supercomputer and on the NERSC supercomputer Carver, and the analysis of the resulting trajectory data was performed on a local cluster in the Head-Gordon lab. Each system was simulated at 300 K, 350 K, 400 K and 450 K, and at 1 atm pressure in the NPT ensemble, or for an NVT ensemble run that was equilibrated in the NPT ensemble at 1 atm. First, thermal equilibration was performed, which for the larger star polymer systems were as long as 50 ns. During equilibration, the partially collapsed star polymer structure collapsed further, and for each system, there were at least 20 Å between sites on neighboring images of polymers in the periodic system, i.e. ~6 or more intervening water layers to reduce direct interaction between copies in different periodic images. After equilibration, production simulations for each of the systems at each given temperature were at least 50 ns.

All simulations were performed using an NVT or NPT ensemble, with thermal control implemented using a Nose-Hoover extended Lagrangian procedure, with a fictitious mass set so as to establish a fluctuation period[18] of approximately 100 fs in the thermostat variable (known as the thermostat damping factor in LAMMPS). The dynamical integration scheme was velocity-Verlet[19] with a timestep of 1 fs. All bond lengths involving hydrogen, as well as the HOH angle for the TIP4P-Ew

model were constrained using a SHAKE[20] procedure, to guarantee that the bond length constraints were satisfied to a tolerance of 10^{-5} Å. Lennard-Jones interactions and direct space electrostatic interactions were truncated at 9.0 Å, and a tail correction for the Lennard-Jones potential beyond this cutoff was included in energy/force and virial pressure calculations. Electrostatic interactions were evaluated with a particle-particle-particle mesh (PPPM) procedure[21] with an accuracy parameter (10^{-5}) that resulted in a 3D k-space grid of 120-by-120-by-120. In accordance with OPLS-AA potential, neither Coulomb nor Lennard-Jones interactions are evaluated for particle pairs that are 1-2 and 1-3 interactions, and both of these interactions are scaled by a factor of 0.5 for 1-4 interactions. Geometric combining rules were used to establish the Lennard-Jones parameters.

Table 3 reports the simulation conditions for each star polymer. For S-POXA (300K, 350K, 400K), L-PEG (350K, 400K), and L-PC1 (350K), the star polymers-water systems were simulated in the NPT ensemble at 1 atm to define an average density, which was then used to set the volume for the production run in the NVT ensemble. The S-PEG system was taken from a previous simulation study[4] that was simulated in the NVT ensemble; in this previous work, the large water box was equilibrated in the NPT ensemble, and then the average volume was set for the NVT run and the star polymer was added (by deleting waters). Although the pressure is higher, we do not expect it to be more than 10atm. Because water is so incompressible, the PV term between 10atm and 1atm is tiny, ~0.005kcal/mole $<<k_BT$, and thus it will have a negligible effect on results. In addition, our study covers a range of temperatures, including high temperatures to improve sampling, although these temperatures are above the boiling point of the water model. As a precaution we set the pressure to 10atm for the L-PEG at 450K and L-PC1 at 400K and 450K, but this will not significantly impair the comparisons to 1atm as explained in above. After the 50 ns of equilibration, production simulations for each of the systems at each given temperature were at least 50 ns (Table 3).

Previous work by Huynh et al. simulated for at least 200 ns per star polymer system at 300K in which they found that most observables were stable after about 15 ns of sampling[22]. Since we are

Analysis: During the simulation runs, the coordinates of all atoms in each system were recorded every 40 picoseconds, allowing for approximately 1250 snapshots for post-processed analysis. As with the previous study[4], structural analysis was performed using in-house software on each star polymer using a variety of shape descriptors, radially averaged mass density, dynamical descriptors, including time orientational autocorrelation functions, and molecular shape information[23] derived from the eigenvalues of the gyration tensor, such as the radius of gyration and anisotropy. When ordered by magnitude from largest (λ_1) to smallest (λ_3), the radius of gyration (R_g), the asphericity (A_{sp}), the acylindricity (A_{cyl}) and anisotropy (A) are computed as follows:

$$R_g = \sqrt{\lambda_1^2 + \lambda_2^2 + \lambda_3^2}$$

$$A_{sp} = \lambda_1 - \frac{\lambda_2 + \lambda_3}{2} \tag{1}$$

$$A_{cyl} = \lambda_2 - \lambda_3$$

$$A = \sqrt{\frac{A_{sp}^2 + \frac{3}{4} A_{cyl}^2}{R_g^2}}$$

A molecule-centered frame of reference was defined from the adamantane core, allowing the polymer system to be characterized without the effect of overall star polymer molecular rotation affecting calculations; thus for each coordinate set, the polymer site vectors and orientations were computed with respect to the molecule-centered reference frame.

Voronoi analyses, as described in the previous study[4], were also performed for each system. A Voronoi analysis[24,25] uses the Cartesian coordinates of every molecule in the system to construct a set of

polyhedra, one surrounding each molecule, that collectively fill the volume of the system. The space enclosed by a molecule's associated polyhedron is closer to that atom that to any other in the system. Polyhedron features shared by multiple polyhedra (faces, edges and vertices) thus represent points equidistant to the molecules corresponding to the polyhedra containing those features. Voronoi analyses are conducted using no additional information besides the Cartesian coordinates of the molecules. However, all the atoms in the system were partitioned into different classes (representing molecular identity, chemical nature, etc.). This allowed us to calculate the volume filled by each class (by summing the volumes of all the polyhedra corresponding to atoms in that class) and the interfacial area between different classes, since neighboring molecules can be easily identified because their associated Voronoi polyhedra share a face. For example, water molecules were grouped into clusters with each cluster representing a contiguous set of neighboring polyhedra, in which the largest of these clusters represents the bulk solvent, while all remaining clusters represent water molecules that have penetrated the interior of the polymer. Similar definitions can be defined for the hydrophobic and hydrophilic segments of the star polymer arms. Because each star polymer was comprised of different chemistry, their total accessible surface areas were not directly comparable. To correct for this fact, a normalization scheme was developed, wherein a fully extended polymer was solvated and initial surface contact areas were calculated between water and each region of the polymer. This number was averaged across all sixteen arms and used as a normalization factor. By normalizing each interfacial area, we could directly compare interfaces between polymers on a range from zero to one. In Table 4, we have reported the normalization factor for each component of the star polymers examined in this paper.

Orientational time correlation functions (OTCF) were computed as follows, and also as described in the previous study[4]. First, a local orientational unit vector, u, was defined for each monomeric unit on each arm of each star polymer. These vectors were directed between specific pairs of atomic sites on each monomeric unit. For PVL the vectors were directed between an alkoxy oxygen

site and the first carbon site immediately opposite the nearest carbonyl group. For PEG, the vectors were directed between pairs of carbon sites, the first and third heavy atoms of each PEG monomer. (Only three vectors were selected within the six-unit PEG part of the chain.) For POXA and PC1, orientational vectors were directed between the first and last heavy atom (non-hydrogen) along the polymer's backbone. Second, for each saved set of coordinates, these vectors were measured and projected from the lab frame onto the molecule-centered reference frame. Third, the time evolution of these vectors in the molecule frame was determined at 40 ps resolution over the 50 ns of the production simulations, and then an autocorrelation function ($<u(0) \cdot u(t)>$) was computed for each monomeric unit. Next, groups of 16 of these functions that correspond to monomeric units at the same position along each of the 16 star polymer arms were averaged. We note that we do not report correlation times, but simply trends, since some of the OTCF profiles decay on timescales not accessible from our simulation.

Monomer-Monomer orientational correlation functions were computed in a similar manner to the OTCFs. The same local orientational unit vectors described above were utilized to compute a correlation function ($<u(n_0) \cdot u(n_i)>$), where n_0 corresponds to a given reference monomer and n_i corresponds to the ith monomer from monomer n_0 along the polymer arm. Finally, the functions were averaged across all polymer arms and across time. For many applications in polymer physics, this correlation may be described with an exponential function that decays with a characteristic length scale, known as the persistence length[26]. Due to the highly structured nature of the polymers studied, we found that the correlations did not fit an exponential decay and we therefore report monomer-monomer orientational correlations.

Hydrogen bonds for the S-PEG and L-PEG system were computed using the HBonds Plugin of Visual Molecular Dynamics (VMD)[27]. The plugin computes the total number of hydrogen bonds between specified types of atoms in the system, in this case between water molecules (hydrogen bond

14

RESULTS

From the principal moments of the gyration tensor, we determined that the shape of all star polymers at all temperatures were found to be nearly spherical, with asphericity measured to be 0.05 or less. Figure S1 reports the temperature trends in the radius of gyration, R_g, for both the inner hydrophobic arms as well as the entire star polymer, for all 4 star polymers considered here. We find that the radius of gyration scales nearly quantitatively based on Flory's mean field approximation in a poor solvent[28], i.e. $R_g \sim N^{1/3}$ when compared between PVL_8PEG_6 and $PVL_{16}PEG_{24}$. The radius of gyration of the hydrophobic segments of the PEG star polymers scale as $2^{1/3}$, consistent with the observed values of 13.2 Å to 13.5 Å for the smaller star polymer compared to the larger star values of 16.7 Å to 17.2 Å, over the complete temperature range. Although the hydrophobic regions are the same between S-PEG and S-POXA and L-PEG and L-PC1, respectively, the hydrophobic regions are slightly more expanded for the POXA and PC1 star polymers.

Correspondingly, the R_g of the complete PEG star polymers scale approximately as $(40/14)^{1/3}$, providing agreement between the measured values of 15.5 Å and 22.0 Å seen for S-PEG and L-PEG, although L-PEG has a weak temperature dependence that is absent for S-PEG that gives deviations of ~2% to larger R_g from the predicted value at 350 K and 450 K. When fully extended, S-POXA should be ~3.8% longer than S-PEG, and its R_g is consistent with that at the coldest temperature, however the POXA polymer shows a temperature trend that increases the R_g beyond the expected scaling. By contrast, while the L-PC1 polymer is expected to be more expanded by ~2.5% compared to L-PEG based on extended length considerations, instead its R_g is smaller by up to ~6% when compared to the large PEG star polymer. These variations in R_g would indicate that the polymer arms have specific chemical interactions that are influencing the observed deviations from idealized polymer behavior.

Voronoi analyses provide an effective method for exploring the frequency of observed contacts made between the hydrophobic and hydrophilic segments of the arms, and the exposure of polymer segments to bulk water. The presence of water clusters separated from the bulk, i.e., interior to the star polymer can also be identified as quantified in Figure 3. If there are multiple water molecules inside the polymer, they may be connected, to form a single cluster, or they may be separate, forming separate interior water clusters. At any given time, a polymer could have no interior water clusters, or it could have one or more interior water clusters, each comprised of a varying number of water molecules. When considering the interior water cluster results, we find that S-PEG does not have any absorbed water ~75% of the time (at 350K), similar to all polymers studied in previous work[4], and when water was absorbed, it was in only 1 or 2 interior clusters. In contrast, S-POXA and L-PEG have some internal water present at least 70% of the simulated time, while L-PC1 always has some internal waters, although for all star polymers the clusters are typically very small, ranging from 1 to 6 water molecules at most. The higher presence of individual water clusters within L-PC1 compared to the other star polymers arises from a complex interaction network of the branched star arms that create small pockets for water to cluster in.

However what is most interesting is where the water clusters reside in the polymer (Figure 4). In contrast to the previous work[4], we present the location of the interior water with respect to the location of the center of mass polymer's adamantane core (previously, the penetration of interior waters was given by a depth, taken with respect to the bulk water; see Figure S3). Given the fact that the polymer regions are on average spherical, we are able to compare water cluster location to the average boundaries of the hydrophobic PVL region and the entire polymer radius, R, computed for a spherical particle as a direct function of our simulated value of R_g. i.e. $R=(5/3)^{1/2} R_g$. Surprisingly, and regardless of size, the PEG polymers have water clusters that intercalcate mostly in the hydrophobic PVL interior, while S-POXA has water at the hydrophobic-hydrophilic interface, whereas L-PC1, which has the most internal water, is concentrated primarily in the hydrophilic outer block.

Temperature does not change the trend in where the interior water is found for any of the star polymers, although higher temperature does increase the frequency of observance of interior water clusters and the corresponding cluster sizes become larger on average (see Figure 3). Although the rough topology of the star polymer may lead one to conclude that the absolute distance of the interior water from the adamantine core could be misleading, we also provide the water cluster neighbor types obtained from the Voronoi analysis, summarized in Table 5, which supports the location of water clusters in each polymer block type.

By contrast, when comparing the degree of interaction of the different star polymers with bulk water, we find that both the hydrophilic arms of S-PEG and L-PEG star polymers are better solvated than the more branched S-POXA and L-PC1 polymers at any temperature, even though the latter star polymers were designed to be more soluble (Figure 5). The PEG star polymers preference for solvent is also manifest in the fact that it increases the PVL-PVL interactions, and shares the least surface area contact with the PVL hydrophobic core, compared to the other star polymers. On the other extreme, PC1 shows significantly stronger polymer-polymer associations, as measured by an increased Voronoi surface area between hydrophilic segments, and evidence that the hydrophilic block overlays and coats the hydrophobic core, likely explaining its reduced R_g relative to L-PEG (Figure 5). In addition both PEG-based star polymers show evidence for decreasing interactions with aqueous solvent and increasing interaction of the hydrophilic arms as temperature increases, supporting the fact that PEG-based star polymers may also be thermo-sensitive like their linear analogues, although we return to this point below. By contrast, the POXA and PC1 polymers have at most a weak temperature dependence, with solubility increasing ever so slightly, over the 350 K to 450 K range (Figure 5a).

Further insight into domain areas of rigidity and flexibility of the four star polymers, and their temperature dependence, is evident in their orientational time correlation function (OTCF) (Figure 6) and orientational correlation function (OCF) between different pairs of monomer units along the polymeric arms. For monomers close to the adamantane core the OTCFs do not decay at all for any

star polymer, however monomer units further out along the arms show rates of decay of their orientational memory that are distinct for each of the star polymers. While the most distant PEG group decays very rapidly for both the small and large polymer, supporting the fluidity of the PEG polymeric block, the monomer ends of POXA and PC1 do not decay on the 2ns upper bound placed on the measured correlation time from our simulations, with POXA showing glassy behavior while PC1 appears to behave as a solid. Furthermore, the OTCF for monomers at the transitional interface between hydrophobic-hydrophilic polymer blocks for both POXA (the 8th PVL and 1st POXA) and PC1 (the 16th PVL and 1st PC1 monomers) remain strongly coupled for all temperatures; in fact the relaxation time for the 1st PC1 monomer is nearly as slow as the 1st PVL monomer near the adamantane core, limiting the reorientations allowed for the central hydrophobic beads of the PVL hydrophobic core. In contrast, we find that for the PEG star polymers that the PVL and PEG monomers, including the transitional regions, are decoupled such that each region along the arm is decaying on its own timescale.

When we analyze the OCF between different pairs of monomer units of the star polymers, we considered two monomer reference points: the hydrophobic bead attached to the adamantane core to measure correlations out to the last hydrophilic bead (Figure 7) and the last hydrophilic bead at the end of the diblock arm to measure correlations back toward the adamantane core (Figure 8). Qualitatively all four star polymers exhibit negative correlations in the hydrophobic arms near the adamantane core, and the oscillations in bond vector directions indicate a complicated folding pattern that never relaxes to the exponential decay of a worm-like-chain model in the hydrophobic region regardless of temperature and length of the PVL block we examined here. However, beyond the transitional region the bond correlations of the 1st PVL monomer with the hydrophilic region shows a decay to zero that is temperature dependent for each star polymer. For S-PEG and S-POXA we find that the OCF with respect to the 1st PVL monomer over the hydrophilic section decays to zero above 300K, whereas for L-PEG the bond correlations decay to zero above 350K. In contrast to the other three systems, over the

350-450K temperature range we simulated for PC1, the bond vectors retain some degree of correlation even at the highest temperature.

These trends are even more dramatic when considering the hydrophilic bead as the reference monomer (Figure 8). In this case both PEG polymers exhibit a OCF that closely approximates 1-2 bond vectors consistent with a freely joined chain above their transition temperature of 300K for S-PEG and 350K for L-PEG, and in the case of L-PEG the temperature transition to uncorrelated bond vectors is striking. However, the OCF for S-POXA is somewhat longer ranged (extending in cases almost to the farthest hydrophilic monomer unit from the arm terminus) than found for the PEG polymers, and furthermore the bond vectors are still weakly correlated in the hydrophilic region even at the highest temperatures. Finally for L-PC1, the evidently strong hydrogen-bonding interactions among the branched hydrophilic arms, and the solid-like nature of motions of the hydrophilic block of the L-PC1 star polymer, shows that the bond vectors remain highly correlated at all temperatures, making the PVL-PC1 diblock combination the least thermosensitive of the star polymers examined here.

The underlying structural origin of the order-to-disorder transition at the melting temperature for the PEG polymers, i.e. as observed in the bond correlation vectors in Figure 8, can be explained by analysis of the dihedral angle populations and PEG-water hydrogen bonding as a function of temperature for S-PEG (Figure 9a) and L-PEG (Figure 9b). The dominant conformation in the aqueous phase is trans (C-O-C-C), gauche (O-C-C-O) and trans (C-C-O-C), TGT, which strongly favors complexation with water and overcomes the unfavorable conformational entropy of this dominant structure and the ordered water network around the polymeric arms. As temperature increases the TGT populations decreases by ~10% while all other conformations (TTT and TGG in particular) increase, resulting in the release of the more ordered water near the PEG surface and a broader distribution in PEG conformations, and a decreased number of PEG-water hydrogen bonds (Figure 9c).

DISCUSSION AND CONCLUSIONS

Biomedical applications of star polymers as a drug delivery system rely on the design of its polymer block chemistries and architectures to be thermosensitive and biocompatible, with the additional ability to be biodegradable over suitable time scales. We note that our star polymer system sizes are relevant for the biomedical applications for which they are designed. Below 400 Da, PEG chains are toxic in humans as a result of sequential oxidation to acid metabolites by dehydrogenases[29]. At the same time, the molar mass should not exceed the renal clearance threshold for complete excretion of the polymer, this limit being in the range of 20-60 kDa for nondegradable polymers[29]. Our systems studied have masses that range from 16-16.5 kDa, and considering that experimental stars have a nanogel core as well, they are at the border of the renal clearance threshold. This means that size effects and degradation studies are quite important as research into star polymers proceeds in the future.

Contrary to our initial hypotheses, increased side-chain branching of the hydrophilic monomers did not increase the hydrophilicity of the POXA and PC1 polymer system, but in fact, decreases polymer-water interactions due to stronger polymer-polymer interactions in the hydrophilic domain. Voronoi interfacial surface area data combined with strong dynamical correlations of POXA and PC1 monomers support these conclusions. With regards to water cluster penetration events, PEG polymers exhibited the most water penetration into the hydrophobic domains, while the extensive level of polymer networking in the PC1 domains provides regions in which small water clusters may reside, and POXA serves as an intermediate between these two extremes. This suggests that the PEG polymers, with their better solvent exposure and greater number of water penetration events into the PVL region compared to the PC1 and POXA polymers, may more readily degrade by hydrolysis, although that degradation may be more limited at higher temperatures. Such analysis is vital considering current research[30-32] on the biocompatibility of PEG and the search for alternatives.

Although PEG-based polymers have been a long industry standard, there are known limitations in synthetic functionalization, and adverse accumulation in the body[19-21], which drive the search for new and competitive biocompatible polymers such as poly-oxazoline[3]. One of the primary conclusions

presented here is that the PEG-based star polymers have structural and dynamical properties that are more sensitive over physiological temperatures than what is observed for the POXA and PC1 star polymers analyzed here. Based on the integrated structural data presented in the results section, we find that the thermodynamic origins of the order-to-disorder transition we observe as temperature increases for PEG star polymers is consistent with entropy-driven dehydration. PEG block regions mix well with water at low temperatures, but exhibit signs of phase separation at higher temperatures, indicating the possibility of a LCST transition, which is observed for linear PEG polymers. At low temperatures the polymeric arms of PEG are dominated by an enthalpically favored TGT conformation, which is stabilized through formation of strong water-ether hydrogen bonds. As temperature increases the entropically favorable release of the ordered water and increased conformational entropy of dihedral angle configurations of the PEG backbone dominate to create a disordered form of the PEG star polymer (see Figure 9).

Although other POXA chemistries have been reported to experience a LCST[33], our analysis of Poly-2-methyl-2-oxazoline agrees with studies indicating the short aliphatic methyl side chain of POXA polymers is insufficient for exhibiting a phase transformation[3], and thus future studies will consider an optimal length for the aliphatic side chains of POXA in the future. POXA is also sensitive to pH which provides another "handle" for structural and dynamical investigations[34]. PC1 is so highly branched and structured that its conformation and interactions with water remain the same across a range of physiological temperatures, indicating that it is least promising in regards drug delivery, and is likely not biocompatible due to hydrogen bond donors that are known to enhance undesirable interactions with surfaces and blood proteins[35], although it may be suitable for alternative applications such as polymer coatings.

While initial theoretical studies in the field of star polymers has begun[4, 22, 36, 37], harnessing the power of various polymer chemistries for use in drug delivery applications will need to explore areas such as drug loading, drug release and biotoxicity. We believe that the LCST in linear and star PEG

polymers and certain POXA polymers may be manipulated for drug delivery systems for finely targeted delivery and degradation mechanisms. Other properties, such as branching and hydrogen bonding sites may also be manipulated to tune polymer behavior for other applications.

SUPPORTING INFORMATION AVAILABLE: Figures for the average radius of gyration for the complete star polymer and the hydrophobic core only, for the orientationally averaged mass density curves for each polymer and depth profiles for interior water clusters are provided below. This material is available free of charge via the Internet at http://pubs.acs.org.

REFERENCES

1. Lee, V. Y., Havenstrite, K., Tjio, M., Mcneil, M., Blau, H. M., Miller, R. D., Sly, J. (2011) Nanogel Star Polymer Architectures: A Nanoparticle Platform for Modular Programmable Macromolecular Self-Assembly, Intercellular Transport, and Dual-Mode Cargo Delivery, *Adv. Mater. 23*, 4509-4515.

2. Appel, E. A., Lee, V. Y., Nguyen, T. T., Mcneil, M., Nederberg, F., Hedrick, J. L., Swope, W. C., Rice, J. E., Miller, R. D., Sly, J. (2012) Toward Biodegradable Nanogel Star Polymers Via Organocatalytic ROP, *Chem. Comm. 48*, 6163-6165.

3. Sedlacek, O., Monnery, B. D., Filippov, S. K., Hoogenboom, R., Hruby, M. (2012) Poly(2-Oxazoline)S--Are They More Advantageous for Biomedical Applications than Other Polymers?, *Macromol. Rapid Comm. 33*, 1648-1662.

4. Swope, W. C., Carr, A. C., Parker, A. J., Sly, J., Miller, R. D., Rice, J. E. (2012) Molecular Dynamics Simulations of Star Polymeric Molecules With Diblock Arms, A Comparative Study, *J. Chem. Theory Comp. 8*, 3733-3749.

5. Saeki, S., Kuwahara, N., Nakata, M., Kaneko, M. (1976) Upper and Lower Critical Solution Temperatures In Poly (Ethylene Glycol) Solutions, *Polymer 17*, 685-689.

6. Horn, H. W., Swope, W. C., Pitera, J. W., Madura, J. D., Dick, T. J., Hura, G. L., Head-Gordon, T. (2004) Development of an Improved Four-Site Water Model for Biomolecular Simulations: TIP4P-Ew, *J. Chem. Phys. 120*, 9665-9678.

7. Jorgensen, W. L., Maxwell, D. S., And Tiradorives, J. (1996) Development and Testing of the OPLS All-Atom Force Field on Conformational Energetics and Properties of Organic Liquids, *J. Am. Chem. Soc. 118*, 11225-11236.

8. Price, M. L. P., Ostrovsky, D., And Jorgensen, W. L. (2001) Gas-Phase And Liquid-State Properties of Esters, Nitriles, And Nitro Compounds With the OPLS-AA Force Field, *J. Comp. Chem. 22*, 1340-1352.

9. Kaminski, G., Duffy, E. M., Matsui, T., And Jorgensen, W. L. (1994) Free-Energies of Hydration And Pure Liquid Properties of Hydrocarbons From the Opls All-Atom Model, *J. Phys. Chem. 98*, 13077-13082.

10. Damm, W., Frontera, A., Tirado Rives, J., And Jorgensen, W. L. (1997) OPLS All-Atom Force Field For Carbohydrates, *J. Comp. Chem. 18*, 1955-1970.

11. Price, D. J., Roberts, J. D., And Jorgensen, W. L. (1998) Conformational Complexity of Succinic Acid And Its Monoanion In the Gas Phase And In Solution: Ab Initio Calculations And Monte Carlo Simulations, *J. Am. Chem. Soc. 120*, 9672-9679.

12. Jorgensen, W. L., And Mcdonald, N. A. (1998) Development of An All-Atom Force Field For Heterocycles. Properties of Liquid Pyridine And Diazenes, *Theochem-J. Mol. Struct. 424*, 145-155.

13. Mcdonald, N. A., And Jorgensen, W. L. (1998) Development of An All-Atom Force Field For Heterocycles. Properties of Liquid Pyrrole, Furan, Diazoles, And Oxazoles, *J. Phys. Chem. B 102*, 8049-8059.

14. Rizzo, R. C., And Jorgensen, W. L. (1999) OPLS All-Atom Model For Amines: Resolution of the Amine Hydration Problem, *J. Am. Chem. Soc. 121*, 4827-4836.

15. Watkins, E. K., And Jorgensen, W. L. (2001) Perfluoroalkanes: Conformational Analysis And Liquid-State Properties From Ab Initio And Monte Carlo Calculations, *J. Phys. Chem. A 105*, 4118-4125.

16. Gontrani, L., Russina, O., Marincola, F. C., And Caminiti, R. (2009) An Energy Dispersive X-Ray Scattering And Molecular Dynamics Study of Liquid Dimethyl Carbonate, *J. Chem. Phys. 131*, 244503.

17. Plimpton, S. (1995) Fast Parallel Algorithms For Short-Range Molecular-Dynamics, *J. Comp. Phys. 117*, 1-19.

18. Martyna, G. J., Tobias, D. J., And Klein, M. L. (1994) Constant-Pressure Molecular-Dynamics Algorithms, *J. Chem. Phys. 101*, 4177-4189.

19. Swope, W. C., Andersen, H. C., Berens, P. H., And Wilson, K. R. (1982) A Computer-Simulation Method For the Calculation of Equilibrium-Constants For the Formation of Physical Clusters of Molecules - Application To Small Water Clusters, *J. Chem. Phys. 76*, 637-649.

20. Andersen, H. C. (1983) Rattle: A "Velocity" Version of the Shake Algorithm For Molecular Dynamics Calculations, *J. Comp. Phys. 52*, 24-34.

21. Hockney, R. W., And Eastwood, J. W. (1989) *Computer Simulation Using Particles*, Taylor & Francis, New York.

22. Huynh, L., Neale, C., Pomes, R., And Allen, C. (2012) Computational Approaches To the Rational Design of Nanoemulsions, Polymeric Micelles, And Dendrimers For Drug Delivery, *Nanomedicine 8*, 20-36.

23. Theodorou, D. N., And Suter, U. W. (1985) Shape of Unperturbed Linear-Polymers - Polypropylene, *Macromolecules 18*, 1206-1214.

24. Brostow, W., Dussault, J. P., And Fox, B. L. (1978) Construction of Voronoi Polyhedra, *J. Comp. Phys. 29*, 81-92.

25. Finney, J. L. (1979) A Procedure For the Construction of Voronoi Polyhedra, *J. Comp. Phys. 32*, 137-143.

26. Grosberg, A. Y., And Khoklov, A. R. (1994) *Statistical Physics of Macromolecules*, AIP Press, New York.

27. Humphrey, W., Dalke, A., And Schulten, K. (1996) VMD: Visual Molecular Dynamics, *J. Mol. Graph. 14*, 33-38, 27-38.

28. Flory, P. J. (1944) Thermodynamics of Heterogeneous Polymer Solutions, *J. Chem. Phys. 12*, 114-115.

29. Knop, K., Hoogenboom, R., Gent, U., Fischer, D., And Schubert, U. S. (2010) Poly(Ethylene Glycol) In Drug Delivery: Pros And Cons As Well As Potential Alternatives, *Angew Chem Int Ed Engl 49*, 6288-6308.

30. Knop, K., Hoogenboom, R., Fischer, D., And Schubert, U. S. (2010) Poly(Ethylene Glycol) In Drug Delivery: Pros And Cons As Well As Potential Alternatives, *Angew Chem Int Ed Engl 49*, 6288-6308.

31. Markovsky, E., Baabur-Cohen, H., Eldar-Boock, A., Omer, L., Tiram, G., Ferber, S., ofek, P., Polyak, D., Scomparin, A., And Satchi-Fainaro, R. (2012) Administration, Distribution, Metabolism And Elimination of Polymer Therapeutics, *J Control Release 161*, 446-460.

32. Barz, M., Luxenhofer, R., Zentel, R., And Vicent, M. J. (2011) Overcoming the PEG-Addiction: Well-Defined Alternatives To PEG, From Structure–Property Relationships To Better Defined Therapeutics *Polymer Chem. 2*, 1900-1918.

33. Diehl, C., And Schlaad, H. (2009) Thermo-Responsive Polyoxazolines With Widely Tuneable LCST, *Macromol Biosci 9*, 157-161.

34. Hoogenboom, R. (2009) Poly(2-Oxazoline)S: A Polymer Class With Numerous Potential Applications, *Angew Chem Int Ed Engl 48*, 7978-7994.

35. Chapman, R. G., Ostuni, E., Takayama, S., Holmlin, R. E., Yan, L., And Whitesides, G. M. (2000) Surveying For Surfaces That Resist the Adsorption of Proteins, *J. Am. Chem. Soc. 122*, 8303-8304.

36. Lee, H., And Larson, R. G. (2009) Molecular Dynamics Study of the Structure And Interparticle Interactions of Polyethylene Glycol-Conjugated PAMAM Dendrimers, *J. Phys. Chem. B 113*, 13202-13207.

37. Lee, H., And Larson, R. G. (2011) Effects of Pegylation On the Size And Internal Structure of Dendrimers: Self-Penetration of Long PEG Chains Into the Dendrimer Core, *Macromolecules 44*, 2291-2298.

38. Soetens, J. C., Millot, C., Maigret, B., And Bako, I. (2001) Molecular Dynamics Simulation And X-Ray Diffraction Studies of Ethylene Carbonate, Propylene Carbonate And Dimethyl Carbonate In Liquid Phase, *J. Mol. Liq. 92*, 201-216.

TABLES

Table 1. *Chemical composition of star polymers studied.* All star polymers have the same hydrophobic block polymer chemistry of PVL = ($-CH_2-CH_2-CO-O-CH_2-$) that is attached to the adamantane core on one end and the hydrophilic block chemistry on the other end, in which the hydrophilic chemistry varies between the star polymers studied. The extension length corresponds to the idealized length of the star polymer arm when torsions are set to 180, which were first collapsed in vacuum and then in aqueous solvent. The collapsed star polymers were then simulated with the amount of solvent yielding somewhere between 4-8 solvation layers around the polymer.

Star Polymer	Name	Hydrophilic region	Extension length (Å)	No. star atoms	No. waters
A[PVL$_8$-PEG$_6$]$_{16}$	S-PEG	PEG = ($-CH_2-O-CH_2-$)	78	2618	45702
A[PVL$_8$-POXA$_6$]$_{16}$	S-POXA	POXA = ($-CH_2-N(COCH_3)-CH_2-$)	81	3194	45483
A[PVL$_{16}$-PEG$_{24}$]$_{16}$	L-PEG	PEG = ($-CH_2-O-CH_2-$)	199	6554	44285
A[PVL$_{16}$-PC1$_{12}$]$_{16}$	L-PC1	PC1 = ($-CH_2-O-CO-O-CH_2-C(CH_3)R-$) R = ($-CO-NH-CH_2-CH_2-OH$)	204	9050	43058

Table 2. *Comparison of charge models for esters using OPLS-AA and for DMC using various approaches.* All charges are in electron units. Soetens charges[38], included for comparison, are fits to electrostatic potentials of lowest energy structure from their HF-SCF (6 - 31G**) calculations. The Soetens charges were also used in the work of Gontrani, et al.

	OPLS (ester)	ESP (water)	ESP (DMC)	Soetens	This work
C (carbonyl)	+0.510	+0.997	+0.963	1.0864	1.000
O (carbonyl)	-0.430	-0.666	-0.633	-0.6774	-0.586
-O- (alkoxy)	-0.330	-0.433	-0.414	-0.4478	-0.414
-C(H2)- (alpha)	+0.190	+0.007	-0.003	-0.1561	+0.105
HC (alpha)	+0.030	+0.087	+0.084	+0.1331	+0.051

Table 3. *Simulation details for star polymer systems.*

Star Polymer	Ensemble	Pressure (atm)	Temperature (K)	Mass density (g/cm^3)	Production Time (ns)
A[PVL$_8$-PEG$_6$]$_{16}$	NVT	-	300	0.9949	57.5
A[PVL$_8$-PEG$_6$]$_{16}$	NVT	-	350	0.9949	54.5
A[PVL$_8$-PEG$_6$]$_{16}$	NVT	-	400	0.9949	53.5
A[PVL$_8$-PEG$_6$]$_{16}$	NVT	-	450	0.9949	59.5
A[PVL$_8$-POXA$_6$]$_{16}$	NPT	1	300	0.9982	48.8
A[PVL$_8$-POXA$_6$]$_{16}$	NPT	1	350	0.9704	53.8
A[PVL$_8$-POXA$_6$]$_{16}$	NPT	1	400	0.9279	56.6
A[PVL$_8$-POXA$_6$]$_{16}$	NVT	-	450	0.9296	64.7
A[PVL$_{16}$-PEG$_{24}$]$_{16}$	NPT	1	350	0.9734	53.4
A[PVL$_{16}$-PEG$_{24}$]$_{16}$	NPT	1	400	0.9308	51.3
A[PVL$_{16}$-PEG$_{24}$]$_{16}$	NPT	10	450	0.8749	54

A[PVL₁₆-PC1₁₂]₁₆	NPT	1	350	0.8925	54
A[PVL₁₆-PC1₁₂]₁₆	NPT	10	400	0.8885	50.4
A[PVL₁₆-PC1₁₂]₁₆	NPT	10	450	0.8367	57.6

Table 4. *Factors utilized in normalization of polymer regions for use in Voronoi interfacial analysis.* Normalization factors were created from a fully extended and solvated star polymer of 16 arms. A Voronoi analysis was performed on the extended structure for each star arm to obtain the total interfacial area between water and each star arm. This value was then averaged to obtain a normalization factor. All uncertainties are ±1 standard deviation.

Polymer region	Normalization factor (Å^2)	Uncertainty (Å^2)
PVL_8	1224.7	17.9
PVL_{16}	2471.6	52.8
PEG_6	413.2	9.7
PEG_{24}	1742.7	30.0
$POXA_6$	708.9	15.5
$PC1_{12}$	3217.3	41.2

Table 5. *Average fraction of interior cluster surface area shared by hydrophobic neighbors for an interior water cluster.* For each interior water cluster, the voronoi analysis provided a list of all neighboring atoms. These neighboring atoms were then sorted into hydrophobic and hydrophilic groups and their interfacial areas between both polymer types were summed and averaged over all interior water clusters observed.

Star type	Fraction of surface area shared with hydrophobic neighbors			
	300 K	**350 K**	**400 K**	**450 K**
S-PEG	0.76	0.88	0.84	0.89
S-POXA	0.55	0.64	0.68	0.74
L-PEG	-	0.88	0.80	0.82
L-PC1	-	0.37	0.42	0.52

FIGURE CAPTIONS

Figure 1. (a) Depiction of the generic diblock star polymer nanoparticle structure when fully extended showing: adamantane core region (yellow), inner hydrophobic polymeric block (blue), and outer hydrophilic polymer block (red). (b) Depiction of the generic star polymer in a partially collapsed state, with same color scheme as (1a). Please note that (a) and (b) are not on the same scale.

Figure 2. Total molecule energy as a function of CT-CT-OS-C torsional angle estimated by both classical and quantum (MP2) methods. Classical results are generated using OPLS-AA parameters.

Figure 3. Histogram of the number of interior water clusters at a given temperature (a) S-PEG, (b) S-POXA, (c) L-PEG, and (d) L-PC1.

Figure 4. The average radius of the complete star polymer (solid marker) and of the hydrophobic core only (smaller value/white marker) as a function of temperature. The black line shows the average water cluster distance from the adamantane core at each temperature (a) S-PEG, (b) S-POXA, (c) L-PEG, and (d) L-PC1. Uncertainty estimates are ±1 standard deviation.

Figure 5. Interfacial area as a function of temperature measured by Voronoi analysis of different diblock regions of the star polymers and water. (a) Interfacial area between the hydrophilic arms and bulk water. (b) Interfacial area within and between hydrophilic arms. (c) Interfacial area between the hydrophilic and hydrophobic (PVL) blocks of the star arms. (d) Interfacial area within and between the hydrophobic (PVL) arms. Uncertainty estimates are ±1 standard deviation.

Figure 6. Orientational time correlation functions as a function of temperature (a) S-PEG, (b) S-POXA, (c) L-PEG, and (d) L-PC1.

Figure 7. Orientational correlation between pairs of monomers as a function of temperature with respect to the reference PVL monomer attached to the adamantane core. (a) S-PEG, (b) S-POXA, (c) L-PEG, and (d) L-PC1. ==Uncertainty estimates are based on the standard deviation in the mean exhibited by the behavior of corresponding repeat units among the 16 arms of each star polymer.==

Figure 8. Orientational correlation between pairs of monomers as a function of temperature with respect to the reference hydrophilic monomer at the end of each polymer arm and moving in toward the adamantane core. (a) S-PEG, (b) S-POXA, (c) L-PEG, and (d) L-PC1. ==Uncertainty estimates are based on the standard deviation in the mean exhibited by the behavior of corresponding repeat units among the 16 arms of each star polymer.==

Figure 9. Dihedral angle distributions for PEG as a function of temperature. (a) S-PEG, (b) L-PEG and (c) Average number of hydrogen bonds per PEG monomer as a function of temperature for both PEG stars.
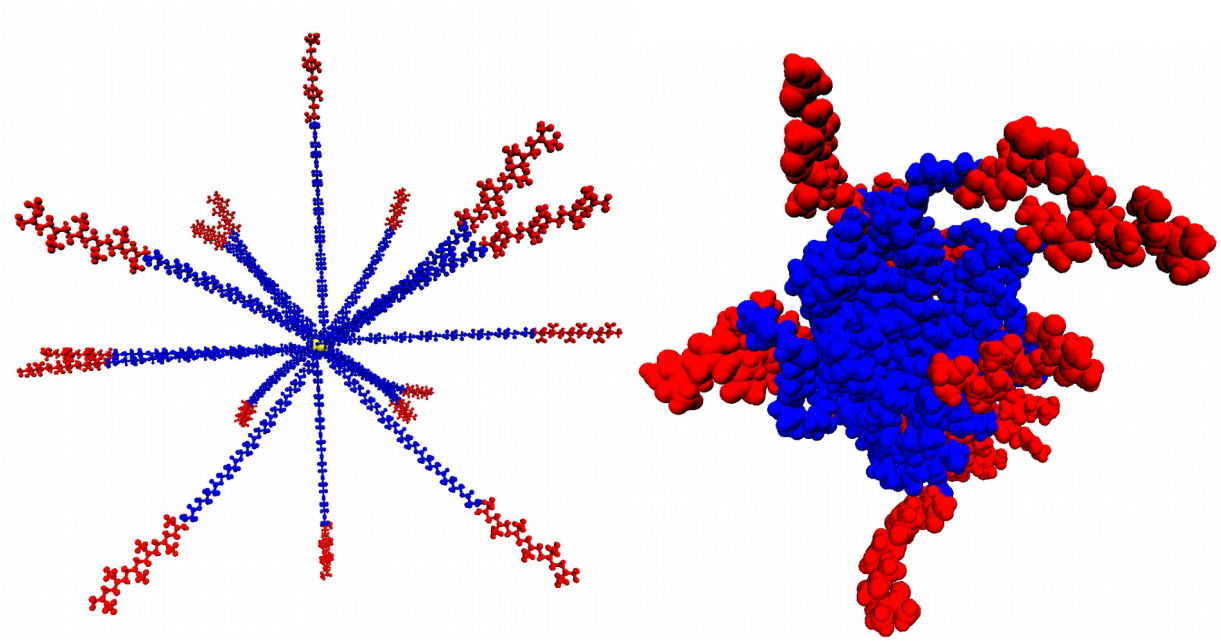
Figure 1. Felberg and Co-worker
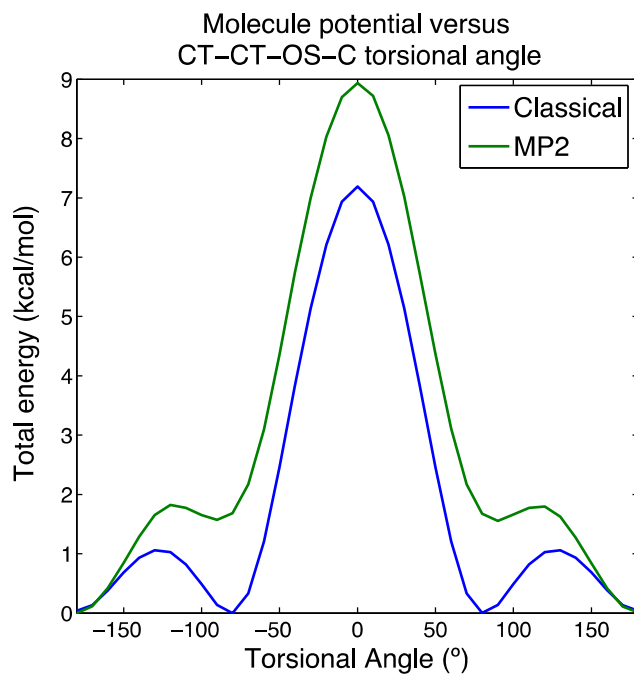
Figure 2. Felberg and Co-worker
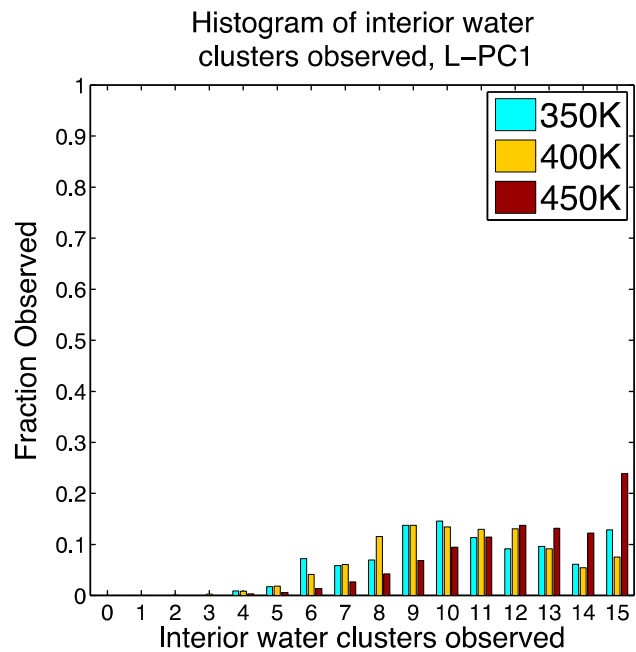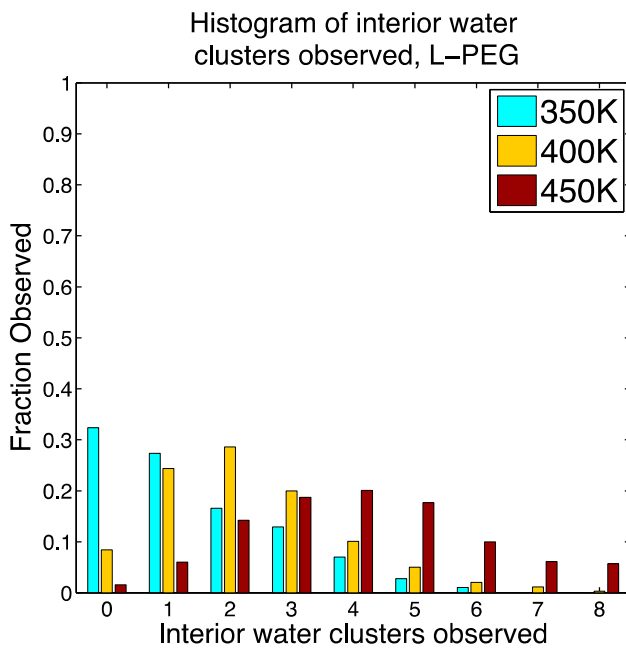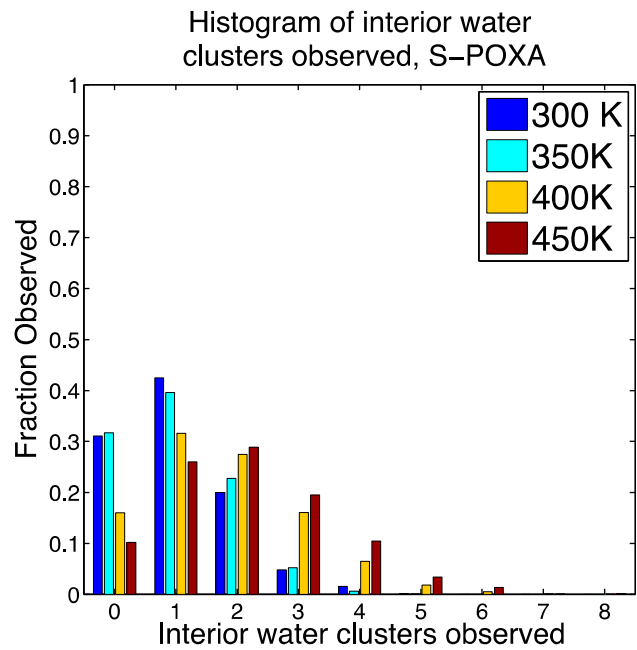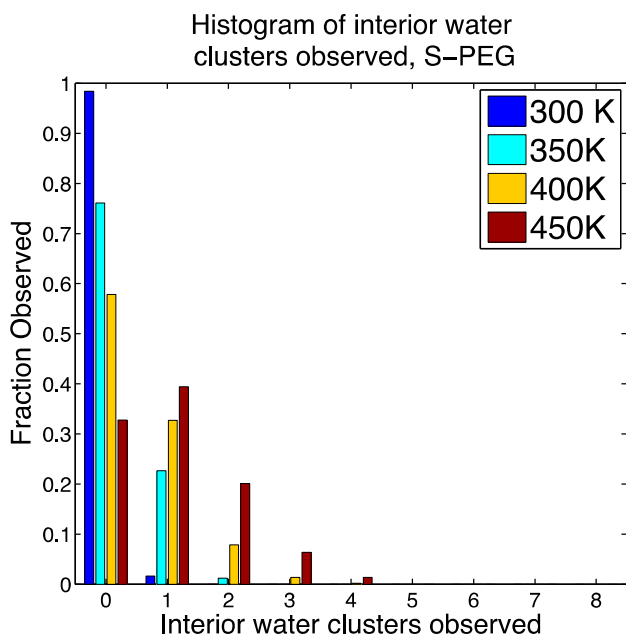
Figure 3. Felberg and Co-workers
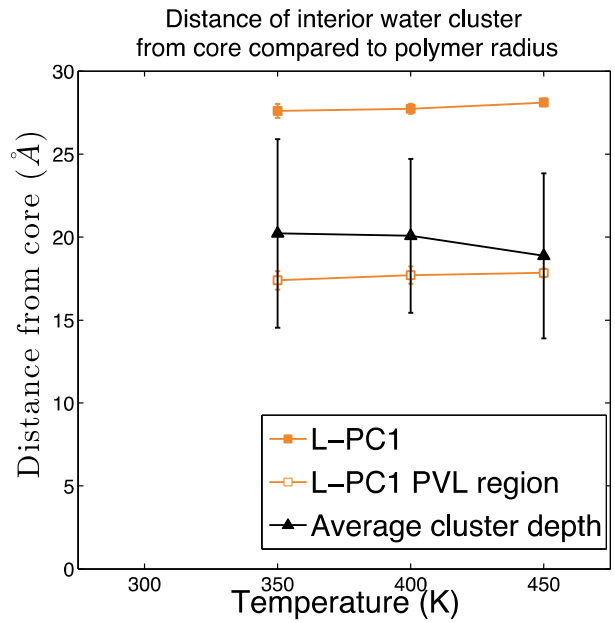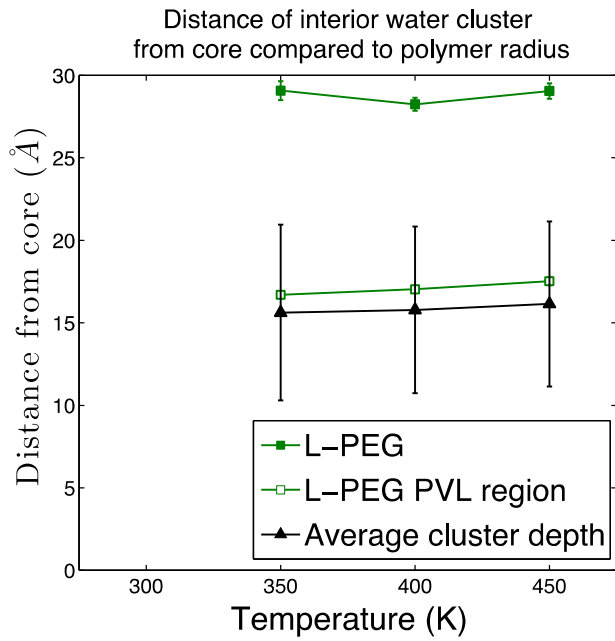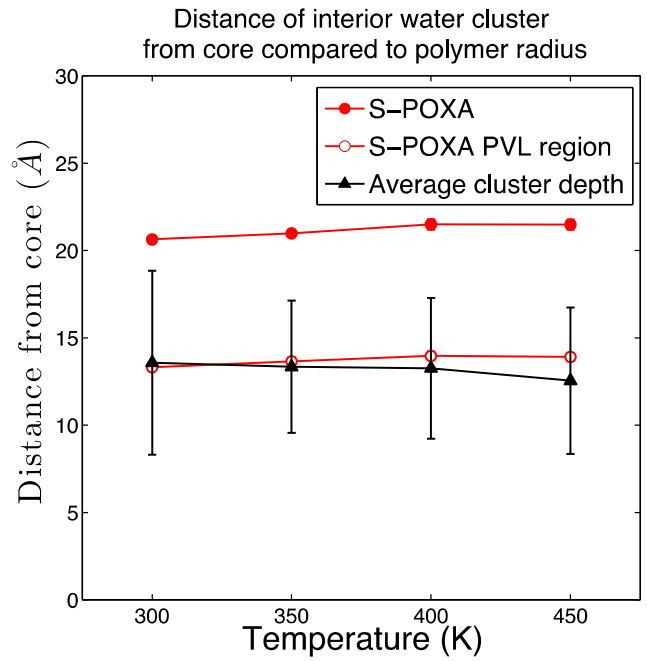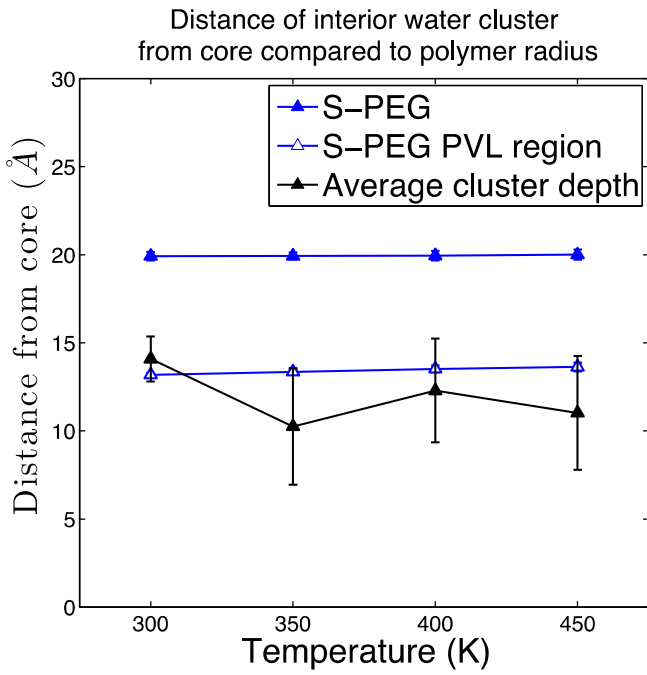
Figure 4. Felberg and Co-workers
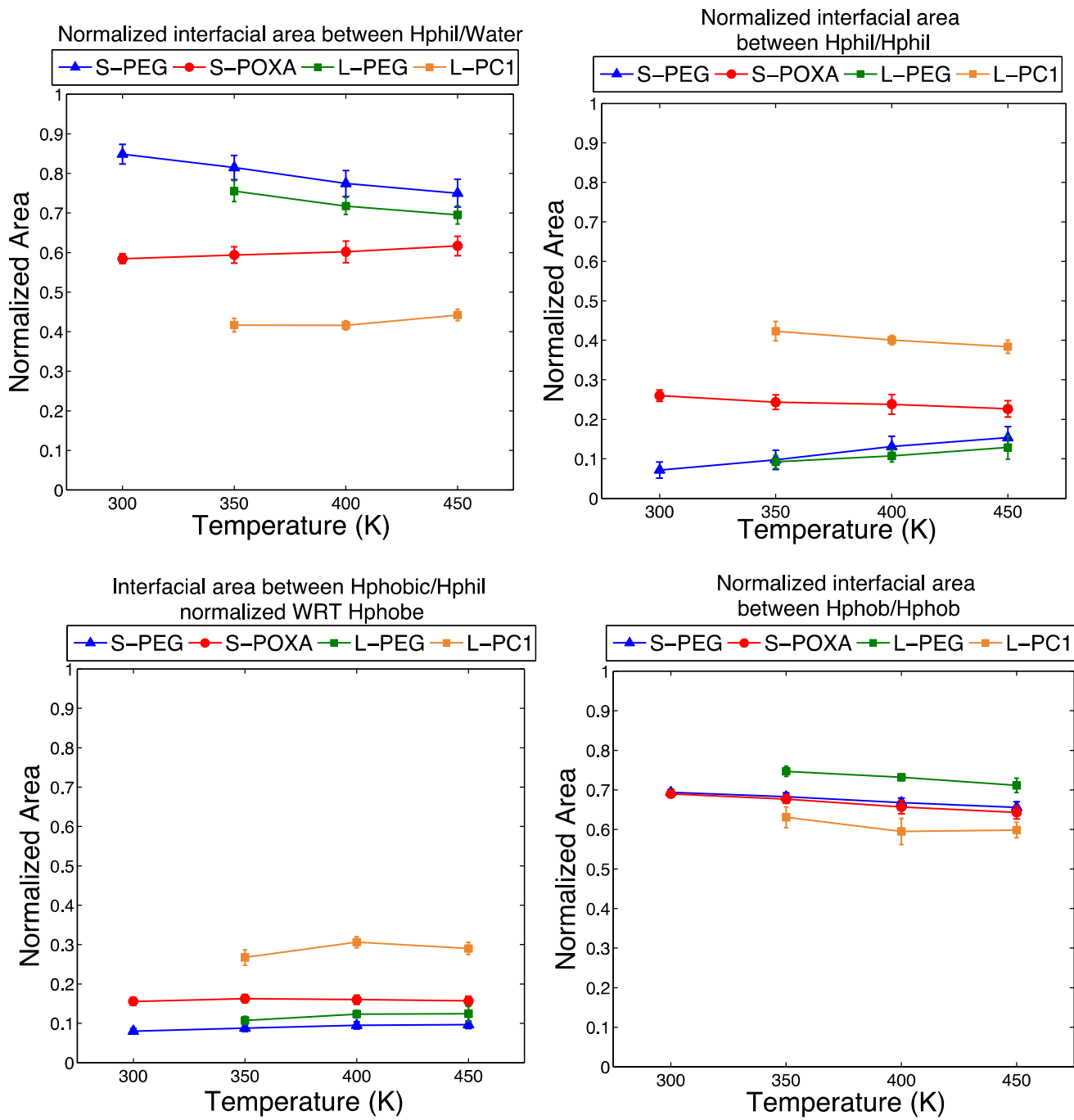
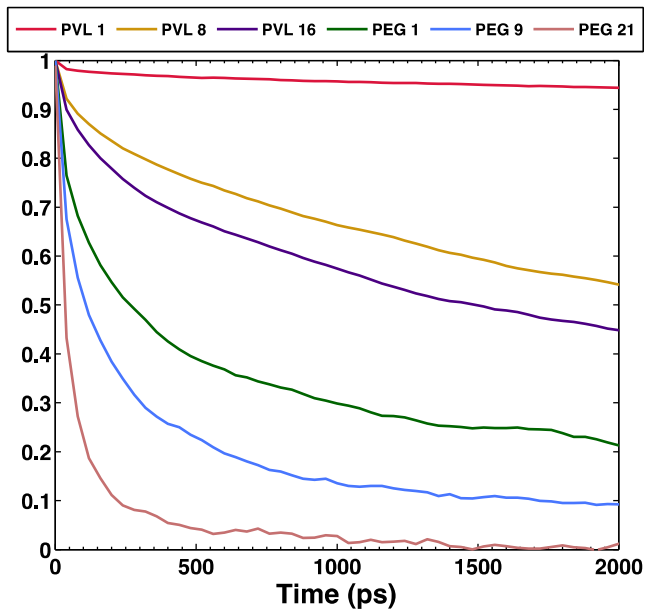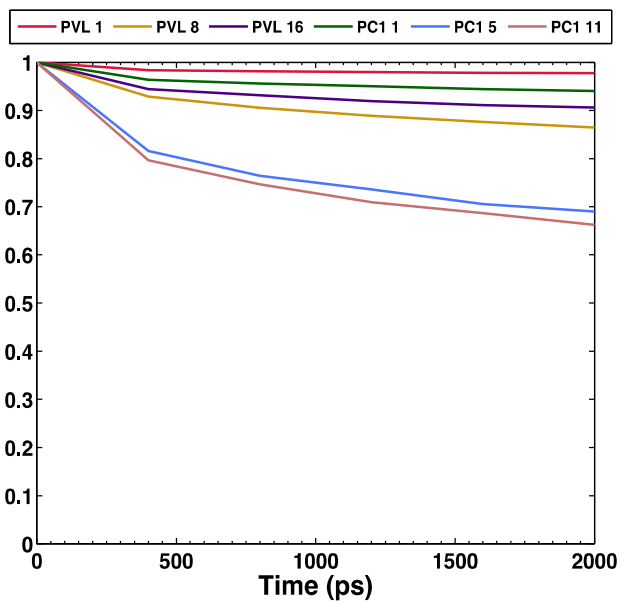**Figure 5. Felberg and Co-workers**
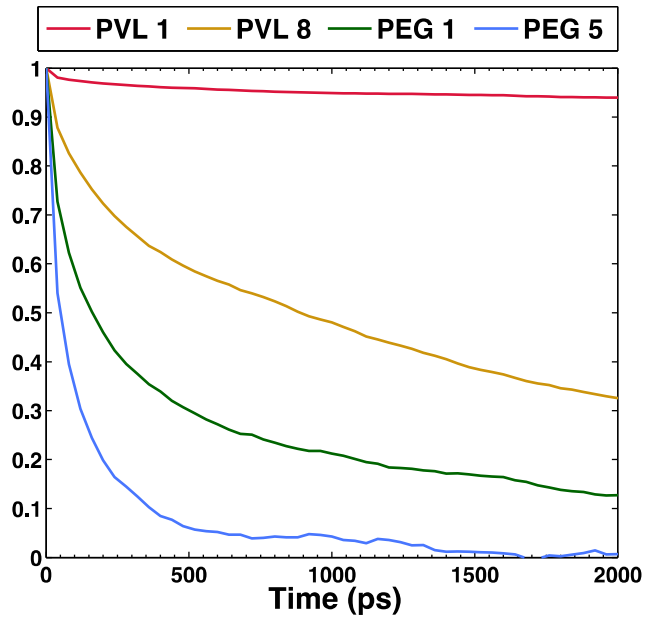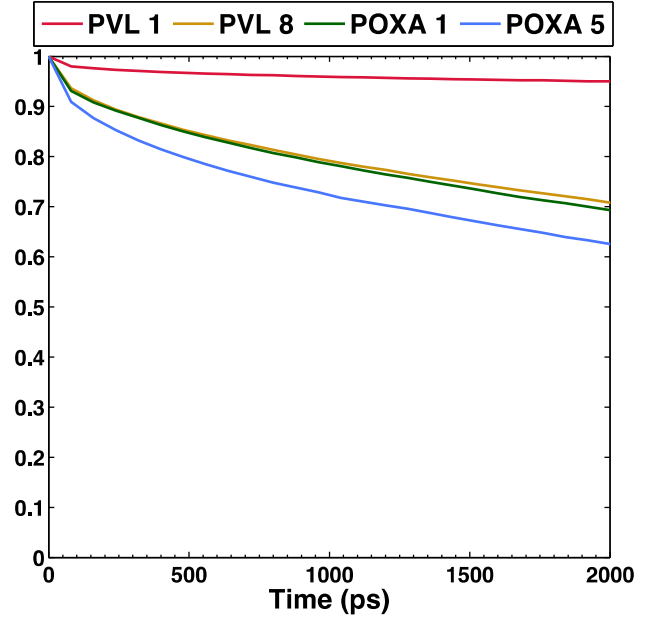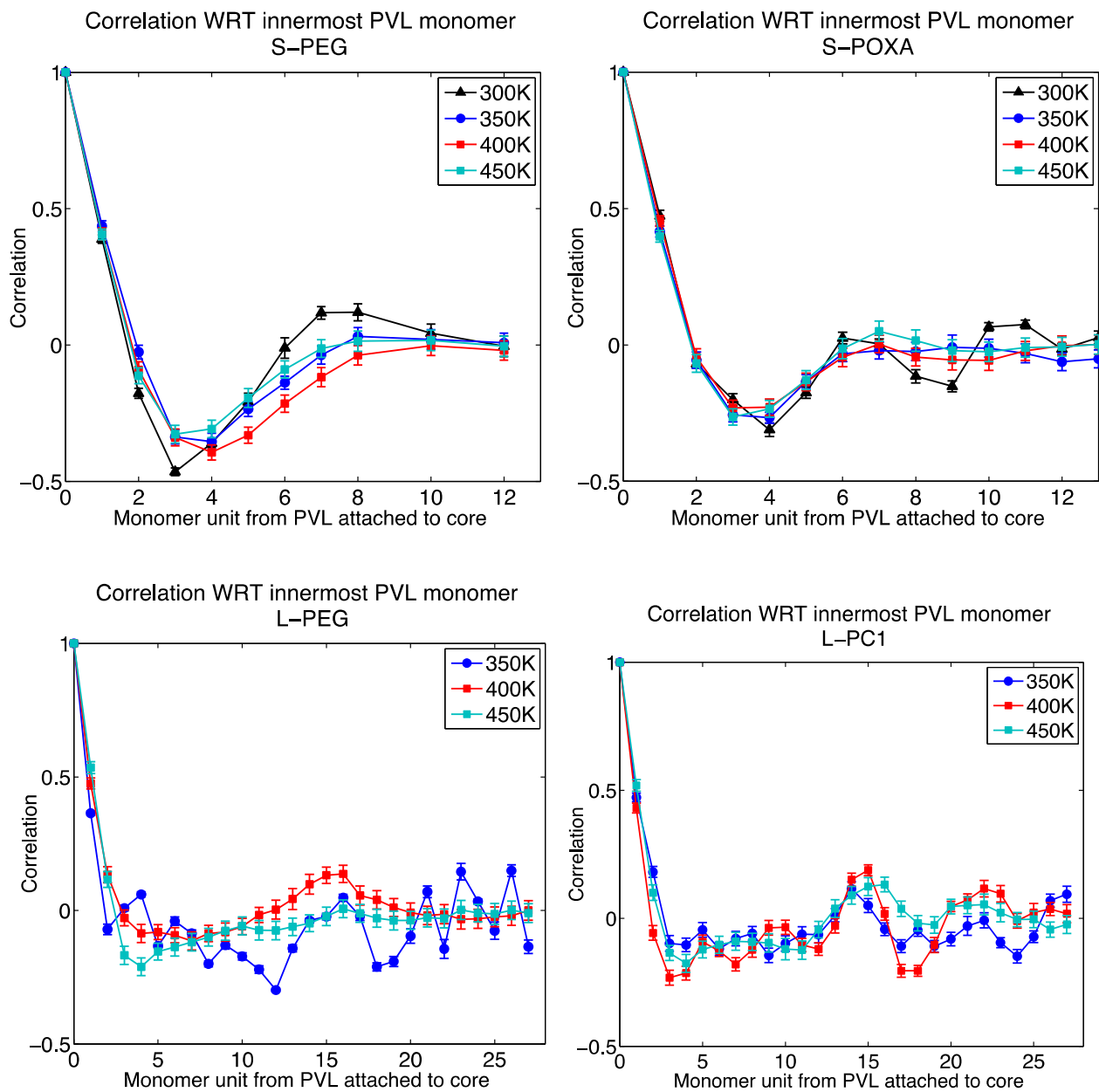
Figure 6. Felberg and Co-workers

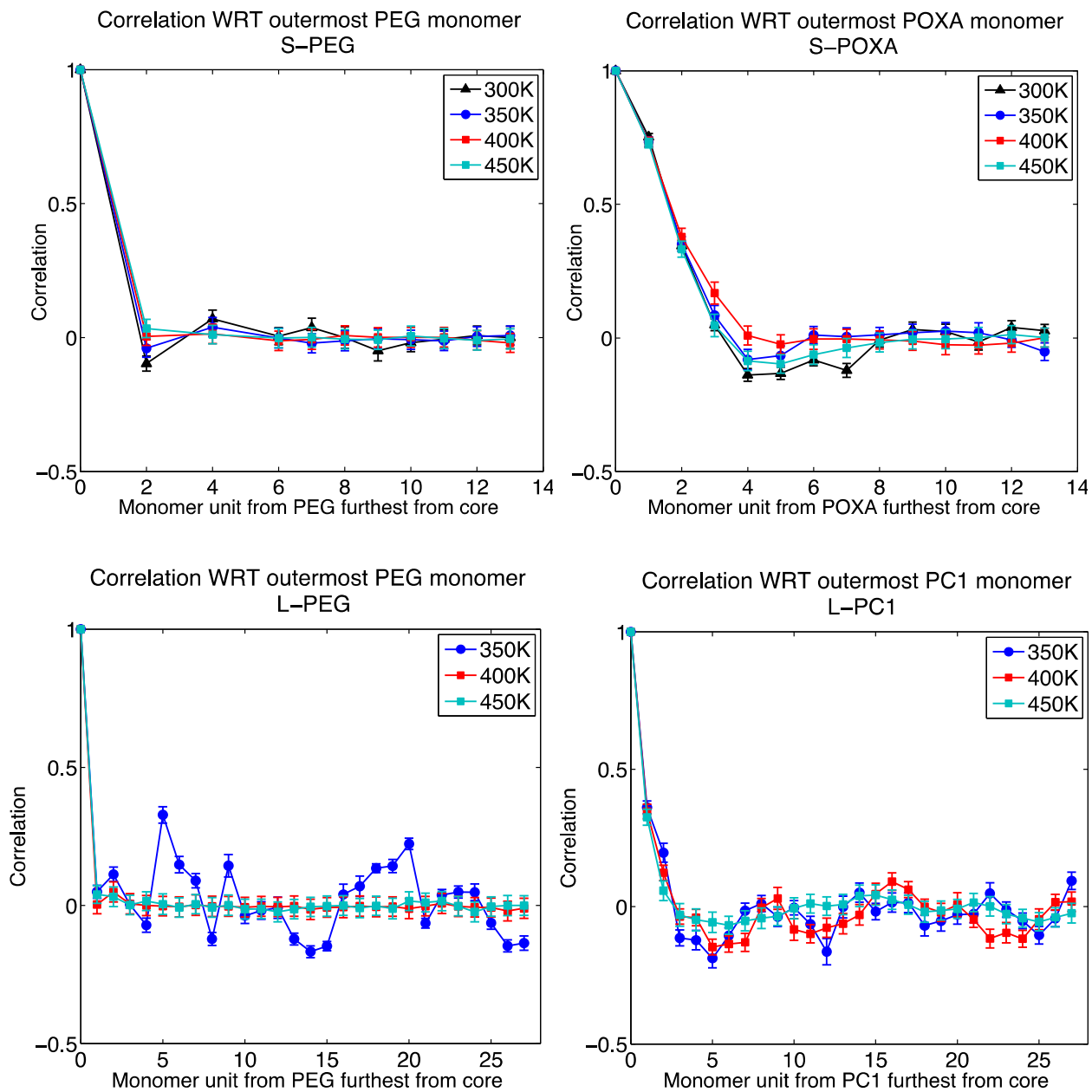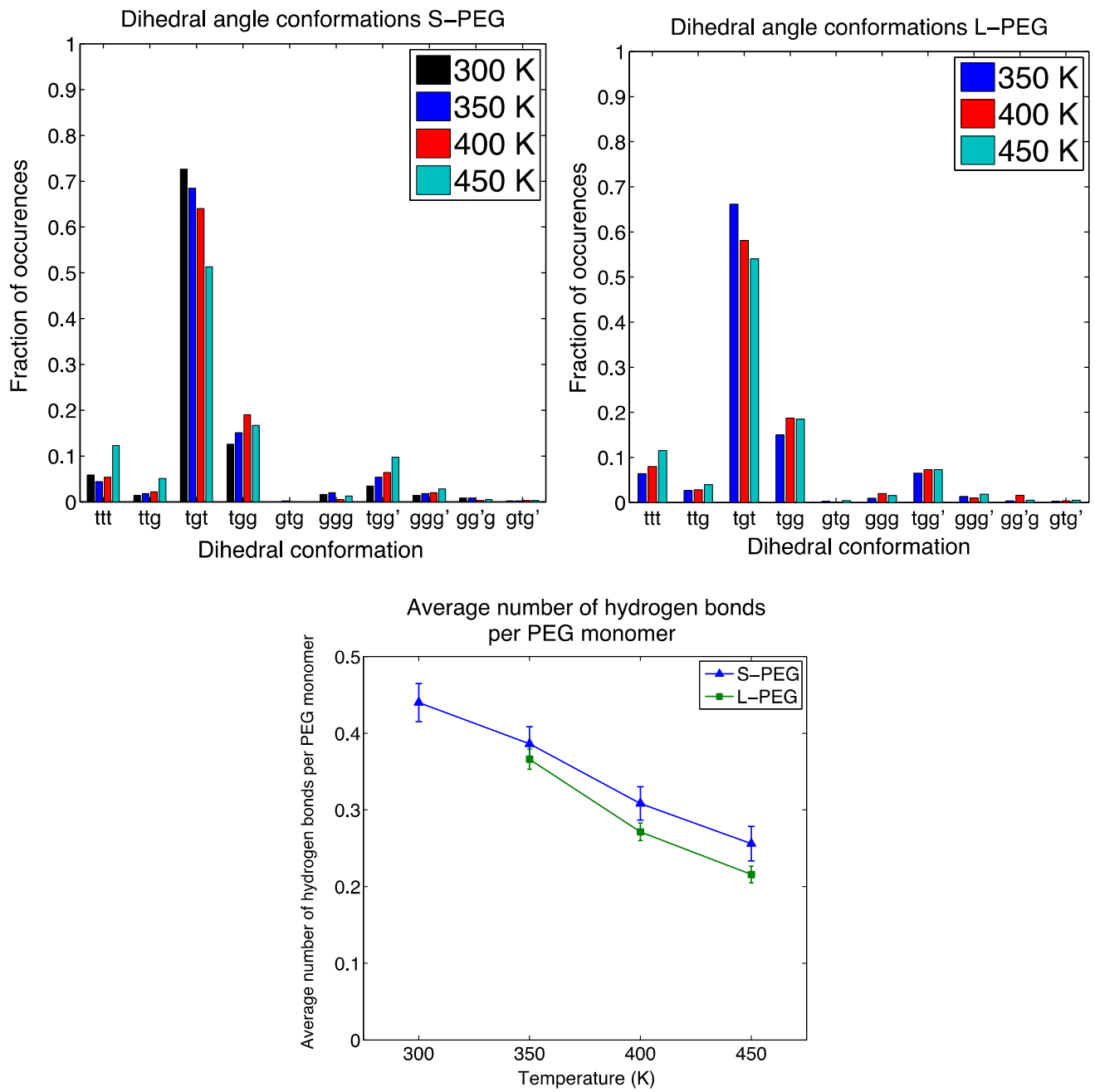**Figure 7. Felberg and Co-workers**

Figure 8. Felberg and Co-workers

Figure 9. Felberg and Co-workers

TABLE OF CONTENTS IMAGE: